Journal of Hydrology 380 (2010) 74–81

Contents lists available at ScienceDirect

Journal of Hydrology

journal homepage: www.elsevier.com/locate/jhydrol

Long-term measurement of stream flow and salinity in a tidal river by the use of the fluvial acoustic tomography system

Kiyosi Kawanisi [a,*], Mahdi Razaz [a], Arata Kaneko [b], Satoshi Watanabe [a]

[a] Department of Civil and Environmental Engineering, Graduate School of Engineering, Hiroshima University, 1-4-1 Kagamiyama, Higashi Hiroshima, Japan
[b] Department of Ocean Atmosphere Environment, Graduate School of Engineering, Hiroshima University, 1-4-1 Kagamiyama, Higashi Hiroshima, Japan

ARTICLE INFO

Article history:
Received 31 July 2009
Received in revised form 12 October 2009
Accepted 18 October 2009

This manuscript was handled by K. Georgakakos, Editor-in-Chief, with the assistance of Attilio Castelarin, Associate Editor

Keywords:
Acoustic tomography
Stream flow
Temperature
Salinity
Tidal channel

SUMMARY

Long-term variation of stream flow of a tidal river was measured by an innovative technology, called the fluvial acoustic tomography (FAT). The reciprocal sound transmission was performed between two acoustic stations, located on both sides of the river. Even in the tidal river with the periodic intrusion of salt wedges, the cross-sectional average velocities along the river stream axis, estimated from the travel time difference data, were consistent with the average velocities, observed by an array of moored downward-looking ADCPs. The cross-sectional average salinity was also estimated by using the mean travel time data collected from the reciprocal sound transmission, the mean values of temperature measured by the conductivity–temperature (*C*–*T*) sensors, and the ray simulation result. The derived salinity data from the FAT are comparable with that obtained by the *C*–*T* sensors.

It is concluded that the fluvial acoustic tomography (FAT) is a prospective method for the continuous monitoring of tidal river discharge and temperature/salinity variations.

1. Introduction

River discharge is an important hydrological factor in river and coastal planning/management and control of water resources. Therefore, it is a key issue to establish the methodology and subsequent technology for measuring stream flow. For continuous measurement of stream flow, a few different methods of instrumentation have been proposed, e.g., acoustic velocity meters (AVMs), horizontal acoustic Doppler current profilers (H-ADCPs), and so on (Catherine and DeRose, 2004; Wang and Huang, 2005). The main drawback of previously proposed methods is that a limited number of velocity sample points are distributed in the cross-section of a river stream, which makes cross-sectional average velocity unreliable. It is difficult to estimate cross-sectional average current velocity in complex flows such as tidal estuaries, or during extreme hydrological events like a flood. In tidal estuaries, the velocity distribution in cross-section is complex and unsteady owing to the intrusion of salt water. As a result, velocities have to be measured at numerous sampling points instantaneously to estimate cross-sectional average velocity accurately. Although several methods to estimate a velocity distribution have been introduced (e.g., by Chiu and Hsu, 2006; Chiu et al., 2005; Maghrebi, 2006), their results are disputable for complicated flow fields as in tidal estuaries with the intrusion of saline water. Thus, an innovative method and/or equipment are still required for continuous high quality measurement of river discharge in tidal estuaries.

In the present study, the fluvial acoustic tomography (FAT) system is proposed as an innovative method to continuously measure the cross-sectional average velocities of tidal rivers, characterized by the intrusion of saline water and the irregular opening of sluice gates. The results of the FAT experiment are compared with those of the ADCP experiment to evaluate the accuracy of the newer FAT.

2. Study area

The Ota River bifurcates into two main branches about 9 km upstream from the mouth as shown in Fig. 1. The upstream border of the tidal compartment in the Ota River estuary is located about 13 km upstream far from the mouth. River flow in this tidal compartment is characterized by the periodic intrusion of salt wedges. The tides are primarily semidiurnal, but mixed with a diurnal component. The tidal range at a spring tide can be as large as 4 m at the mouth. The observation site was located 246 m downstream from

* Corresponding author. Tel./fax: +81 82 424 7817.
E-mail addresses: kiyosi@hiroshima-u.ac.jp (K. Kawanisi), mahdirazaz@hiroshima-u.ac.jp (M. Razaz), akaneko@hiroshima-u.ac.jp (A. Kaneko), s.watanabe5510@gmail.com (S. Watanabe).

0022-1694/$ - see front matter © 2009 Elsevier B.V. All rights reserved.
doi:10.1016/j.jhydrol.2009.10.024

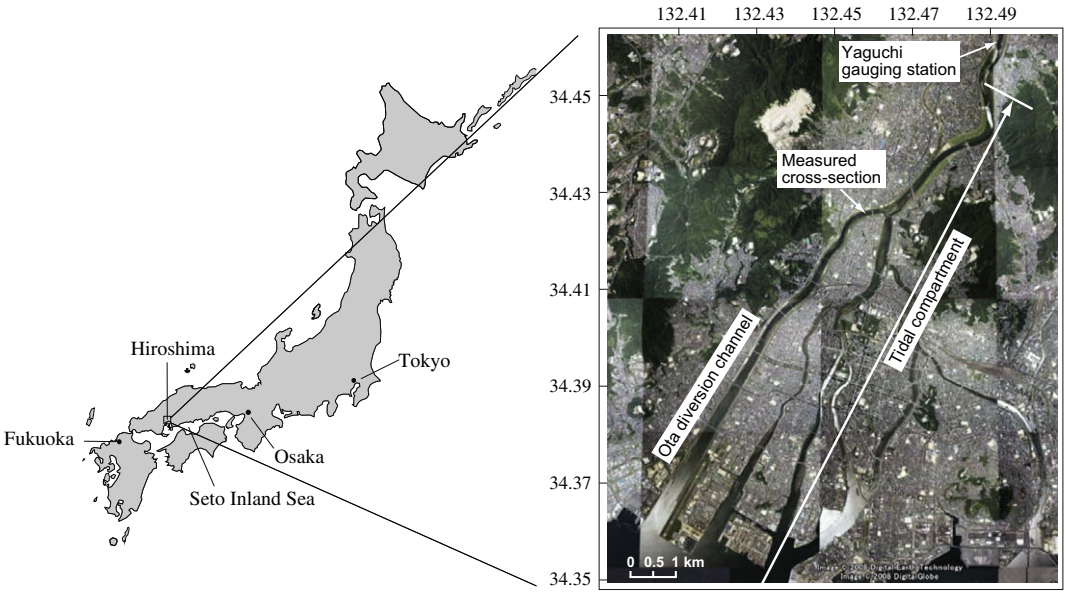

Fig. 1. Study area and experimental site.

the Gion sluice gates near the branched region (Fig. 1). The Ota diversion channel at the observation site is 120 m wide with a bed slope of about 0.04%, and the water depth varies in a range from 0.3 m to 3 m depending on tidal phases. A salt wedge is formed in the ebb tide due to the tidal straining (Simpson et al., 1990).

The freshwater runoff into the diversion channel is usually controlled by the array of Gion sluice gates, located near the bifurcation place. Usually only one sluice gate is opened slightly in order to make the stream cross-section of 32 m $\times$ 0.3 m for spilling water. The inflow discharge is about 10—20% of the total flow rate of Ota River in normal days. However, the accurate discharge at the Gion sluice gates is indefinite because the flow is influenced by tidal oscillation and saltwater intrusion. During flood events, all sluice gates are completely opened and the freshwater runoff from the Gion sluice gates is designed to be about half the total river discharge. Since the flow at the Yaguchi gauging station, which is located in 14 km upstream from the mouth, is not tidally modulated, the Ota River discharge before the bifurcation can be estimated by the rating curves. The saline water in this estuary can intrude up to as far as 11 km upstream from the mouth.

3. Method

3.1. Overview of the system

As shown in Fig. 2, in this method a couple of transducers are on both sides of the channel to measure velocity component along the sound transmission line (ray path). The FAT system measures the

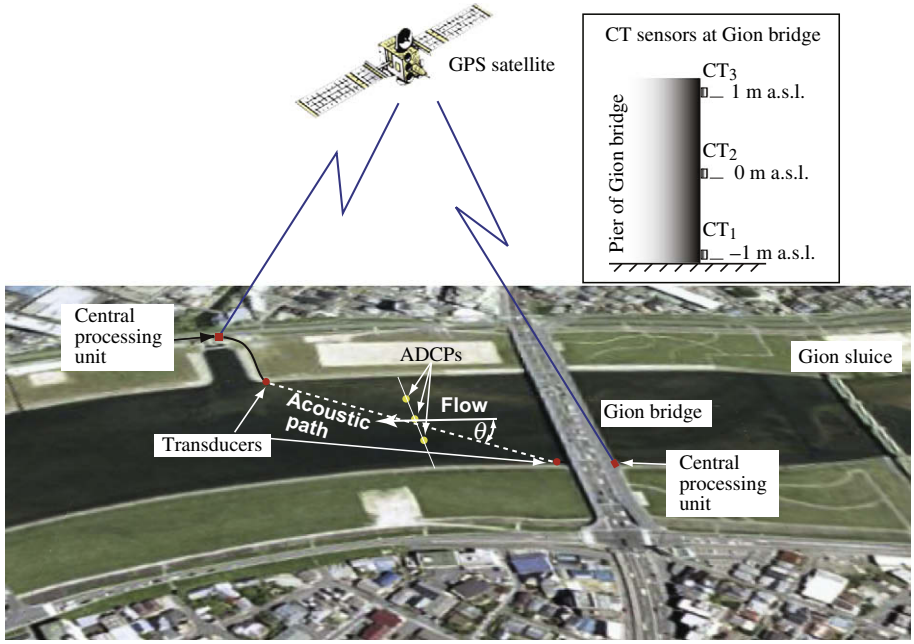

Fig. 2. Aerial view of the experimental set-up.

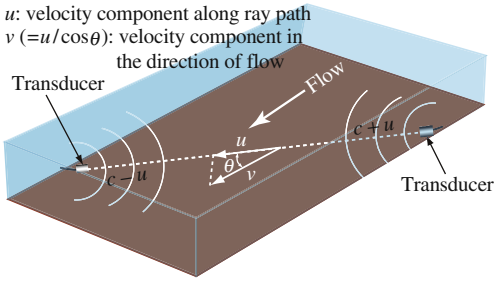

Fig. 3. Velocity component along ray path u, velocity component in the direction of flow v, and ray-path angle θ; $v = \frac{u}{\cos\theta}$.

range-averaged velocity along a ray path. As shown in Fig. 3, the velocity component in the direction of flow v is estimated from the velocity component along the ray path u. Other characteristics of the FAT system are listed as: (a) the central frequency of broadband transducers is 30 kHz, (b) the angle between ray path and stream direction θ is 30°, (c) the transducers are mounted at the height of 0.2 m above the bottom, the altitudes of upstream and downstream transducers are -0.46 ± 0.01 m.a.s.l and -0.7 ± 0.01 m.a.s.l ,respectively, (d) sound pulses of the FAT system are simultaneously transmitted from the omni-directional transducers every minute at a timing synchronized with a GPS clock.

Three moored ADCPs (Aquadopp profiler, Nortek AS) are used to validate the discharge data obtained from the FAT system. As shown in Fig. 2, the ADCPs are arranged at 30 m transverse intervals with the central ADCP put at the centerline of the river. The ADCPs are operated at 2 MHz and 18 Hz pinging rates. Three ADCP transducers, which are equally spaced at 120° azimuth angles, transmit a beam oriented 25° off the vertical axis. The bin length is set to 0.1 m, the interval of ensemble average to 120 s, and the profiling interval to 300 s. The accuracy of horizontal velocity is as large as 0.028 m/s. The blank zone of ADCP measurement near the water surface is 0.22 m in thickness while that near the bottom is estimated by $d(1 - \cos 25°) + 0.1$ m, where d is the distance from the depth of ADCP transducer to the bottom.

Water level and vertical distribution of temperature and salinity are measured every 10 min by the conductivity–temperature (C–T) sensors, attached to the pier of the Gion Bridge at 40 m from the left bank (Fig. 2). The cross-sectional distribution of temperature and salinity is measured by the successive CTD casts from the Gion Bridge. Transverse spacing of the CTD casts is set to 20 m and it takes about 10 min to complete the traverse.

The channel bathymetry along the transmission line was surveyed (with an accuracy of 0.01 m) on 17th March 2008. Examples of river cross-sections are shown in Fig. 4.

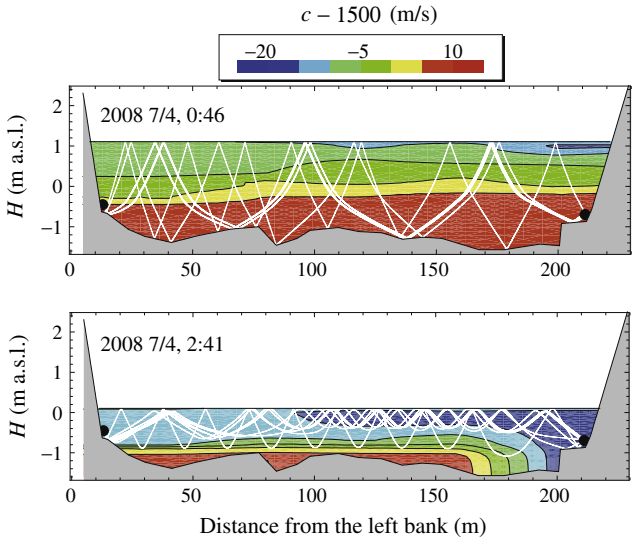

Fig. 4. Examples of river cross-sections, contour plots of sound speed distribution and the results of ray simulation (ray pattern). The cases for the transducer, put inside and above the salt wedge are shown in the upper and lower panels, respectively. The rays with bottom reflection numbers greater than five are not shown here.

3.2. Measurement principles and error analysis

Measurement principle of the FAT is similar to that used in an acoustic velocity meter (AVM). Namely the range-averaged velocity along the transmission line is calculated by using "time of travel method" (Sloat and Gain, 1995). In fact, the FAT system is able to estimate the cross-sectional average velocity using the multi ray paths that cover a stream section. If measuring only one component of velocity field leads to reliable flow rate estimation, the FAT system may be operated with just a couple of transducers. A four-station system with two crossing transmission lines is required otherwise (e.g., for meandering rivers).

Let us consider two acoustic stations, placed at horizontal spacing L in a fluid medium moving with velocity u_m. The travel times t_1 and t_2 for the forward and reverse directions are calculated by the following formulae

$$t_1 = \frac{L}{c_m + u_m} \tag{1}$$

and

$$t_2 = \frac{L}{c_m - u_m} \tag{2}$$

respectively. From Eqs. (1) and (2) the sound speed c_m and water velocity u_m averaged along the sound path are given by

$$c_m = \frac{L}{2}\left(\frac{1}{t_1} + \frac{1}{t_2}\right) \approx \frac{L}{t_m} \tag{3}$$

$$u_m = \frac{L}{2}\left(\frac{1}{t_1} - \frac{1}{t_2}\right) \approx \frac{L}{2}\frac{\Delta t}{t_m^2} = \frac{c_m^2}{2L}\Delta t \tag{4}$$

where $t_m = \frac{t_1+t_2}{2} \approx t_1 \approx t_2$, and $\Delta t = t_1 - t_2$.

By taking the total differentiation of Eqs. (3) and (4), the relative errors of c_m and u_m are estimated as

$$\frac{\delta c_m}{c_m} = \frac{\delta L}{L} - \frac{\delta t_m}{t_m} \tag{5}$$

$$\frac{\delta u_m}{u_m} = \frac{\delta L}{L} - 2\frac{\delta t_m}{t_m} + \frac{\delta(\Delta t)}{\Delta t} \tag{6}$$

respectively. The average travel time errors δt_m and $\delta(\Delta t)$ are negligible when both systems are synchronized precisely with the GPS clock. As a result, the relative error of the average sound speed $\frac{\delta c_m}{c_m}$ and the relative error of the average velocity $\frac{\delta u_m}{u_m}$ are equated to the relative error of the horizontal distance $\frac{\delta L}{L}$. Concerning Eq. (6), the right term is negligible only if the time accuracy is radiant, i.e. $\delta(\Delta t)$ is insignificant.

3.3. M-sequence modulation

In order to accurately identify the arrival time of traveling sound mixed with noises, the transmitted signal is phase-modulated by applying the pseudo-random sequence (Simon et al., 1985; Zheng et al., 1998). Fig. 5 shows the transmission signal modulated with the 3rd order M-sequence as a typical example.

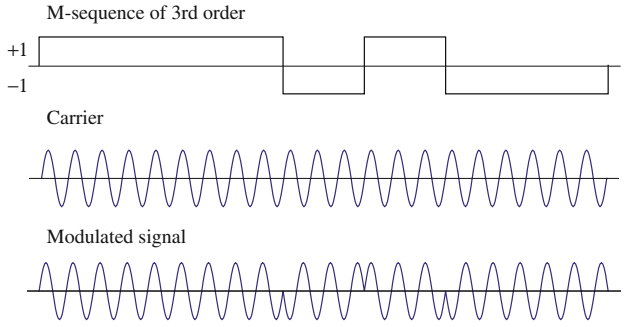

Fig. 5. Phase-modulation of carrier signals by the 3rd order *M*-sequence.

The carrier signal is phase-modulated by taking a product with the *M*-sequence. By transmitting this modulated signal with a broadband frequency range, the signal-to-noise ratio (SNR) is increased remarkably. In this study, the higher order (10th order) *M*-sequence is applied to get higher SNRs, increasing with $(2^n - 1)$ where n denotes the order of *M*-sequence.

The transmission signal with a phase-modulation is expressed by

$$s(t) = M(t)A(t)\sin(\omega t) = A(t)\sin[\omega t + \psi(t)] \tag{7}$$

where $A(t)$ and $\psi(t)$ are the amplitude and phase functions, respectively. The angular frequency ω is set to 30 kHz in the present study. The received signal $S(t)$ is processed using the *M*-sequence of 10th order, i.e. the cross-correlation between the received signal and the *M*-sequence. This process serves to identify the precise arrival time.

3.4. Ray tracing simulation

In order to estimate the cross-sectional average velocity, sound paths are expected to traverse a larger stream section between the bottom and surface of the flow. If the sound speed has an inhomogeneous distribution in the section, sound rays draw curves obeying Snell's law of refraction. In this paper, ray simulation is implemented by solving the following differential equations (Dushaw and Colosi, 1998):

$$\frac{d\varphi}{dr} = \frac{\partial c}{\partial r}\frac{1}{c}\tan\varphi - \frac{\partial c}{\partial z}\frac{1}{c} \tag{8a}$$

$$\frac{dz}{dr} = \tan\varphi \tag{8b}$$

$$\frac{dt}{dr} = \frac{\sec\varphi}{c} \tag{8c}$$

where φ is the angle of ray measured from the horizontal axis r, z is the vertical coordinate, and t the time. Here, the sound speed c is estimated by Medwin's formula (Eq. (9)) as a function of temperature T (°C), salinity S, and depth D (m) (Medwin, 1975):

$$c = 1449.2 + 4.6T - 0.055T^2 + 2.9\times10^{-4}T^3 + (1.34 - 0.01T)(S-35) + 0.016D \tag{9}$$

Notice here that presently we do not need to notify [psu] as a salinity unit, i.e. the practical salinity adopted by the UNESCO/ICES/SCOR/IAPSO Joint Panel on Oceanographic Tables and Standards does not have dimension. The total differentiation of sound speed δC reduces to:

$$\delta c = \{4.6 - 0.11T + 8.7\times10^{-4}T^2 - 0.01(S-35)\}\delta t + (1.34 - 0.01T)\delta s = \alpha\delta T + \beta\delta s \tag{10}$$

In Fig. 6, the coefficient α , which indicates sensitivity to the temperature, is plotted against T with parameter S. Another coefficient β, which indicates sensitivity to salinity, is plotted against T in Fig. 7. The sound speed is more sensitive to T rather than S. The sensitivity of sound speed to T is 2.5—4.5 times greater than that to salinity. At $T = 15$ °C and the possible range of S, α reaches about 3.5 while β is about 1.2.

The cross-sectional average sound speed c_m is expressed by

$$c_m = 1449.2 + 4.6T_m - 0.055(T_m^2 + \widehat{T'^2}) + 2.9\times10^{-4}T_m(T_m^2 + 3\widehat{T'^2}) + (1.34 - 0.01T_m)(S_m - 35) - 0.01\widehat{T'S'}) + 0.016D \tag{11}$$

where T_m and S_m are the cross-sectional average temperature and salinity, respectively, and means cross-sectional average and $'$ denotes the deviation from it.

The c_m is not sensitive to the variance $\widehat{T'^2}$ and covariance $\widehat{T'S'}$ of the deviations as seen in Eq. (12):

$$\delta c_m = \alpha\delta T_m + \beta\delta S_m + (-0.055 + 8.7\times10^{-4}T_m)\delta(\widehat{T'^2}) - 0.01\delta(\widehat{T'S'}) \tag{12}$$

Note α and $\beta \gg (-0.055 + 8.7\times10^{-4}T_m)$ and 0.01. Hence, further attention is not paid to $\widehat{T'^2}$ and $\widehat{T'S'}$ in the following sections.

4. Results and discussion

The ray simulation, observed results of flow velocity, and river discharge are presented together in this section. The ADCPs data are used to validate the flow velocity and river discharge from the FAT system. Then, the flow temperature and salinity that deduced from processing sound speed (mean travel time) data and

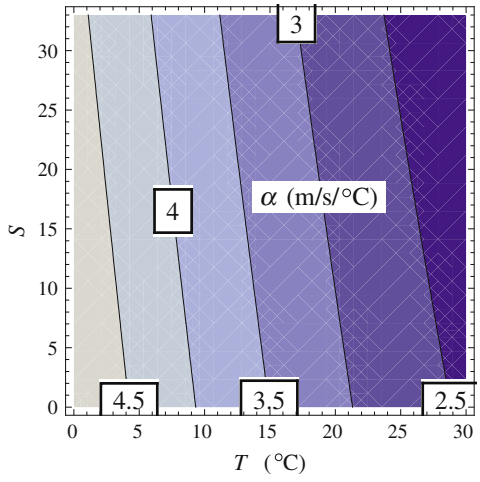

Fig. 6. Sensitivity diagram of sound speed to water temperature.

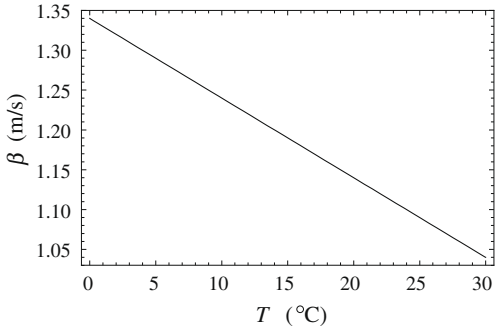

Fig. 7. Sensitivity diagram of sound speed to salinity.

collected by the FAT system, are compared to those acquired from the conductivity–temperature sensors (*C–T* sensors).

4.1. Correcting the cross-sectional average velocity

The FAT system is intended to measure the cross-sectional average velocity of the river stream. Then the ray pattern is preferable to cover the cross-section as much as possible. However in a two-layer estuary with maximum salinity difference ΔS_G of 20, all rays emitted from a transducer in the upper layer will finally be confined in the upper layer. These rays would not be able of penetrating into the lower layer with a reverse flow, as shown in Figs. 4b, 8 and 9.

In Fig. 4, the ray patterns immediately after the high water slack (HWS) and immediately before the low water slack (LWS) are presented as typical examples of ray simulation. The sound speed was calculated by Medwin's formula, applying the results of the CTD casts which were executed from the Gion Bridge. In ray simulation, the effect of velocity is negligible compared to that of sound speed. In the rivers with a salt wedge, salinity increases with depth and forms a two-layer system such as what happened in the observation site. The sound speed varied from 1510 m/s in the lower layers to 1480 m/s in the upper layers.

The rays with bottom reflection numbers greater than five are not shown in Fig. 4. They correspond to rays released at larger angles from the horizontal at the source position. Mostly, the ray paths cross approximately all the sections as illustrated in Fig. 4a. Unfortunately, at a period with a near-bed intrusion of salt wedge, the sound rays emitted in the upper layer are reflected at the underlying interface and prevented from penetrating into the lower layers (Fig. 4b). In this case, the cross-sectional average velocity is significantly overestimated by the FAT system since it cannot cover all the cross sections. The ray tracing simulation suggests that the correction is required when the salinity difference ΔS_G between the upper and lower layers exceeds eight in the configuration with the transducer above the density interface.

Fig. 9 demonstrates the vertical profile of salinity obtained from *C–T* sensors and the velocity profile measured by the ADCP; located at 40 and 30 m away from the left bank, respectively; over the strong stratification period. The velocity profiles in a stratified flow may be predicted by Eq. (13) (Shima et al., 1964):

$$\frac{u}{U_u} = a_i\left(\frac{z}{h_u}\right)^2 + b\left(\frac{z}{h_u}\right) + c \quad (i = 1, 2) \tag{13}$$

where U_u is the average velocity in the upper layer,

$$a_1 = -\frac{6}{4+3K}, \quad a_2 = \frac{9}{\{K(4+3K)\}}, \quad b = \frac{12}{4+3K},$$
$$c = \frac{12}{4+3K}, \quad K = \frac{h_l}{h_u}$$

where the h_u and h_l are depths of the upper and lower layer, respectively. The red curve in Fig. 9 represents the profiled predicted by this equation.

When the picnocline is established below the transducer, the average velocity measured by the FAT system is equivalent to the

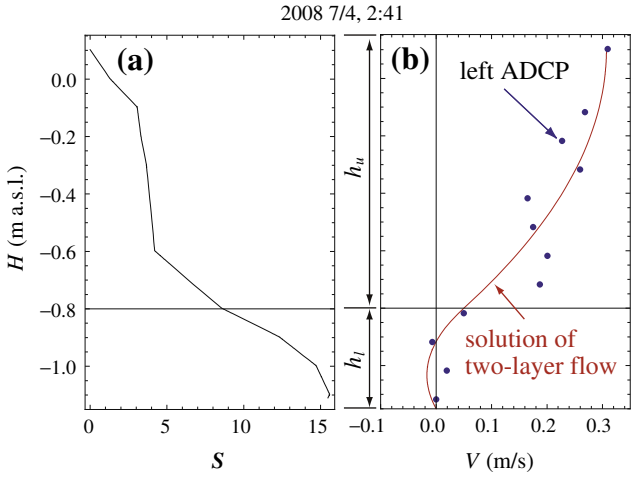

Fig. 9. Vertical profiles of (left panel) salinity at 40 m away from the left bank and (right panel) velocity from the left side ADCP at the intrusion of salt wedge.

average velocity of the upper layer $U - u$. This means that the FAT system somewhat overestimates the cross-sectional average velocity. From Eq. (13) the depth average velocity is deduced to:

$$U = \frac{1}{6(h_u + h_l)}\left[2a_1 h_u + \frac{2a_2 h_l^3}{h_u^2} + 6c(h_u + h_l) + b\left(3h_u - \frac{3h_l^2}{h_u}\right)\right]U_u \tag{14}$$

Following Eq. (14), we can correct the average velocity if the depth of picnocline is known. In the present study, h_l is estimated by the following equation:

$$h_l = \frac{S_1 - 0.4(S_1 + S_2)}{S_1 - S_2} - 0.35 \tag{15}$$

where S_1 and S_2 are the salinities at altitudes of −1 m.a.s.l and 0 m.a.s.l.

Although the above correction can be applied to two-layer flows with a salt wedge, the correction is probably not needed in most sites. The corrections are needed in particular sites that have strong salinity gradients as seen in the present site. However, the correction is not needed if the transducers are located inside the salt wedge because the sound rays can be refracted easily in the upper layer with a slower sound speed. Obviously, the correction is no longer needed in rivers without saltwater intrusion.

4.2. Temporal variation of water discharge

The water discharge is calculated by the following formula:

$$Q = A(H)v_m \sin\theta = A(H)u_m \tan\theta \tag{16}$$

where $A(H)$ is the cross-sectional area in which sound makes ray paths, v_m is the cross-sectional average velocity and θ is the angle between the ray path projected to the horizontal plane and stream axis. The cross-sectional average velocity measured by the FAT

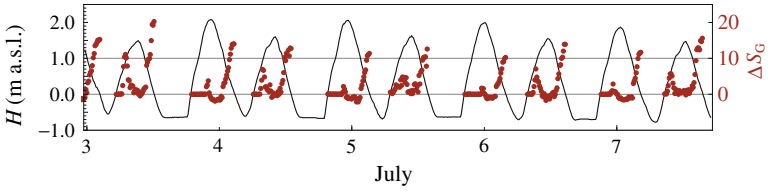

Fig. 8. Time plots of water level and salinity difference between the altitudes of −1 m and 0 m.

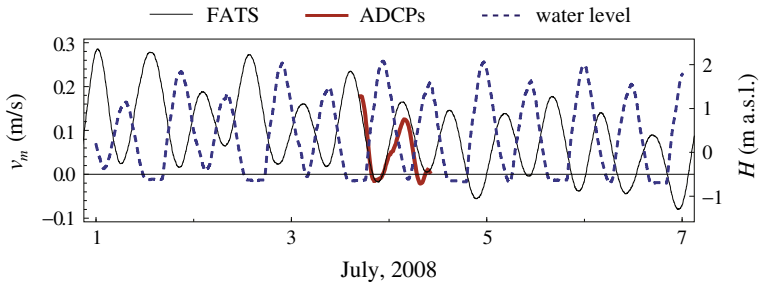

Fig. 10. Comparison of the cross-sectional average velocities obtained from the FAT system (black solid line) and arrayed ADCPs (thick red solid line). The water level data is also shown with the blue broken line. (For interpretation of the references to colour in this figure legend, the reader is referred to the web version of this article.)

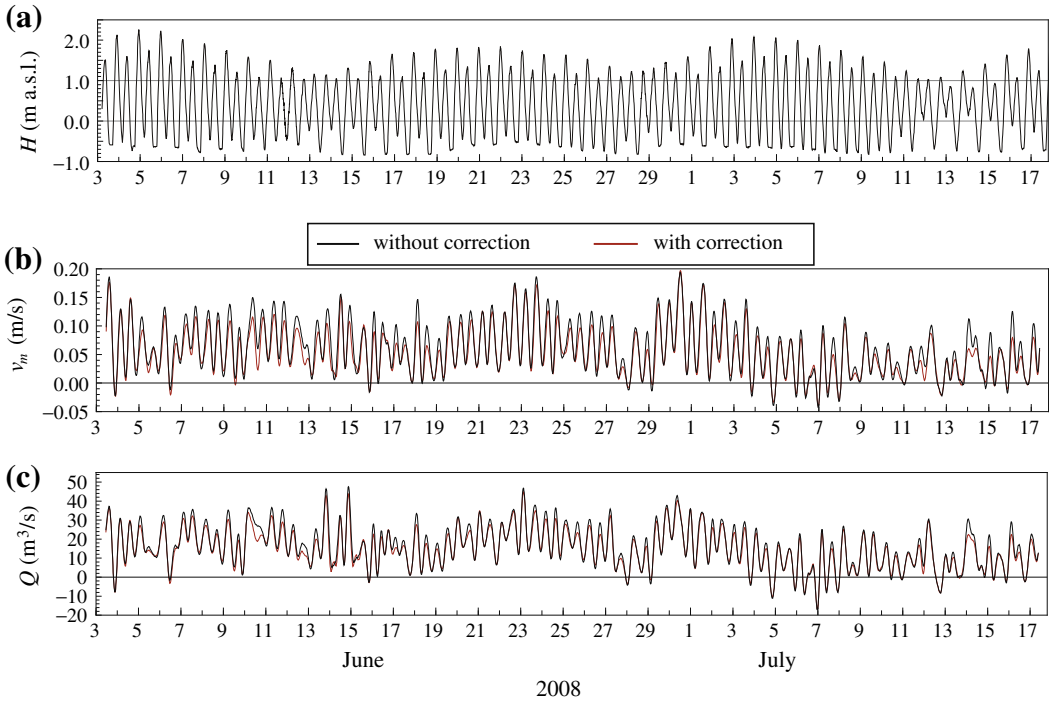

Fig. 11. Time plots of (a) water level, (b) cross-sectional average velocity and (c) river discharge for one and half months. The black and red lines are used for data before and after the discharge correction, respectively. (For interpretation of the references to colour in this figure legend, the reader is referred to the web version of this article.)

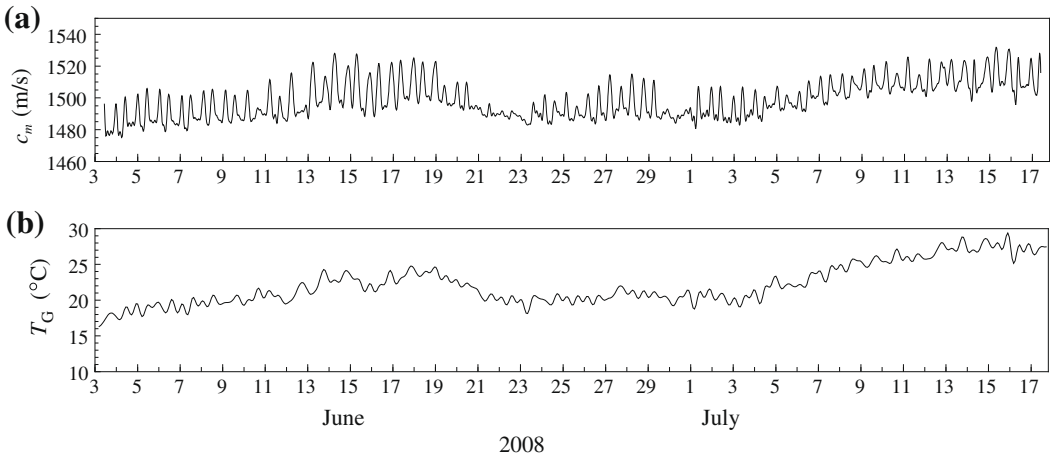

Fig. 12. Power spectral diagram of the river discharge variation.

system is compared with the arrayed ADCP result in Fig. 10. Both velocities are analogous. Moreover, the interrelationship between the FAT-derived average velocity and the water level is reasonable, i.e., the velocity and water level are out of phase each with other and the velocity amplitude increases with the tidal range. Unfortunately, we cannot correctly discuss the accuracy of the FAT system in velocity measurement in comparison with the ADCP result, because the average velocity estimation from the three-ADCP data is unreliable to some extents. This problem stems from the fact that the tidal flow was inhomogeneous, forming a complex stream field, and the spacing of the moored downward-looking ADCPs was too large to estimate the cross-sectional average velocity correctly. However, comparing the ADCP data at three points with the continuous FAT data supports that the cross-sectional average velocities obtained from the FAT system are comparable/close to the actual river flow velocity.

The 44-day variations of water level, cross-sectional average velocity and flow discharge are shown with the time plots in Fig. 11. The corrected values of discharge, designated by the red lines, are smaller by about 10% on average over the observation period than those without correction. The discharge variation in the observation site is dominated by tidal variations such as semi-diurnal and diurnal tides and disturbed significantly by unknown factors. This is mainly caused by the discharge control of the Gion sluice gates to reduce inflow into the observation site. Fig. 12 shows the power spectral diagram of discharge variation. The prominent diurnal and semi-diurnal peaks are visible in the spectral diagram.

The long-term measurement of cross-sectional average velocity and river discharge is successfully performed by the FAT system even in an estuary with a salt wedge intrusion. It is, thus, suggested that the present FAT system is a prospective method for the continuous measurement of the river discharge.

4.3. Temporal variations of the cross-sectional average sound speed, water temperature and salinity

The cross-sectional average sound–speed measured by the FAT system and the depth-averaged water temperature by the conductivity–temperature (C–T) sensors are presented with the time plots in Fig. 13. It is noticeable that the sound speed trend is similar to that of water temperature. The relationship between the daily

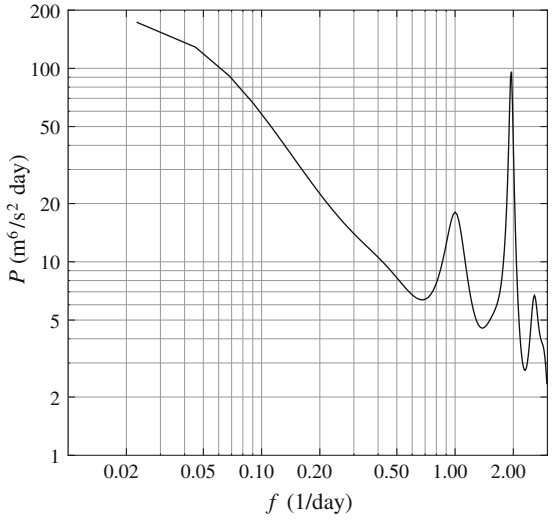

Fig. 13. Time plots of (a) the FAT-derived cross-sectional average sound–speed and (b) the depth average temperature obtained at Gion bridge.

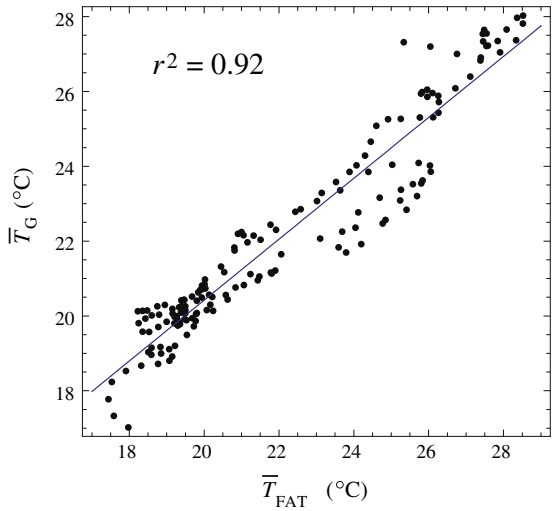

Fig. 14. Regression diagram of the temperature ($\overline{T}_G$) obtained from the C–T sensors, plotted against the FAT temperature ($\overline{T}_{FAT}$). The coefficient of determination ($r^2 = 0.92$) is presented at upper left of the figure.

mean water temperatures deduced from the FAT system and the C–T sensors at the Gion Bridge is provided in Fig. 14. The water temperature from the FAT system is obtained by using the salinity, averaged over the observation period. It is evident that the FAT-derived temperature and the temperature from the C–T sensors are well correlated.

As shown in Figs. 5 and 6, the water temperature has larger influence on the sound speed than the salinity. Accordingly, sound speed increases mainly with water temperature. However, in a tidal river with intrusion of a salt wedge, the variation of salinity is more predominant than that of temperature. Therefore, the first priority of research is transferred to salinity rather than temperature. We shall here focus on the salinity variation.

The effect of sound path length variations on the variation of cross-sectional average salinity is given by:

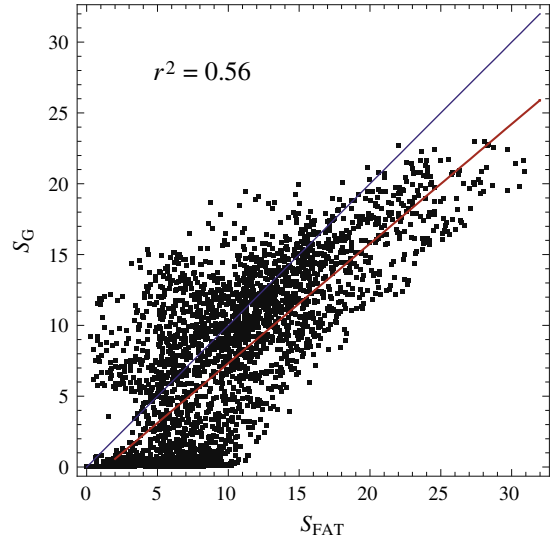

Fig. 15. Regression diagram (red line) of the salinity ($\bar{S}_G$) obtained from the C–T sensors, plotted against the FAT salinity ($\bar{S}_{FAT}$). The 1:1 line is shown with the blue line. The coefficient of determination ($r^2 = 0.56$) is presented at upper left of the figure. (For interpretation of the references to colour in this figure legend, the reader is referred to the web version of this article.)

$$\delta S_m = \frac{c_m}{(1.34 - 0.01T_m)} \frac{\delta L}{L} \quad (17)$$

Substituting the ray tracing simulation results into Eq. (15) δS_m is evaluated about 5. Fig. 15 shows the regression diagram of the average salinity S_{FAT} calculated from the FAT data and the salinity S_G obtained from the submerged *C–T* sensors. There is a significant, positive correlation between S_{FAT} and S_G, although the data are scattered from the regression line. The scattering is probably caused by the sound path length changes and the difference of sampling points between the FAT system and *C–Ts*. Actually, the sampling section of the FAT system placed downstream of the *C–T* location (the location of the transducer at the right bank is 174 m downstream from the Gion Bridge). The red line denotes the regression line presented by:

$$S_G = -1.11 + 0.844 S_{FAT} \quad (18)$$

This indicates a potential ability of the FAT system to measure cross-sectional average salinity in tidal rivers. The ratio of S_{FAT} for S_G is smaller than 1 ($S_{FAT} > S_G$) because of the FAT sampling section placed downstream of the *C–T* location. There are some data points, showing $S_{FAT} < S_G$. This anomaly, caused by the inability of sound paths to penetrate into the bottom layers, is a consequence of salt water intrusion to a depth below the transducer level.

5. Conclusions

The fluvial acoustic tomography (FAT) system, characterized by the GPS precise clock system and the *M*-sequence modulation of transmission signals was developed and applied to a shallow tidal river with intrusion of salt water. The FAT system is composed of a couple of acoustic transducers, located on both sides of a channel and sound transmission line between them is arranged at an angle of about 30° to the channel axis in order to enable the measurement of the cross-sectional average velocity. The signal-to-noise ratio of the received signals was remarkably improved by the signal transmission, phase-modulated by the 10*th* order *M*-sequence. The FAT system is asserted as a powerful tool to measure river discharge even under flood events with high turbidity concentration and large ambient noise levels of sound.

The long-term measurement of the cross-sectional average velocity and river discharge were carried out successfully in spite of the periodic intrusion of a salt wedge into the river. It is concluded that the fluvial acoustic tomography (FAT) is a prospective method for the continuous monitoring of tidal river discharge.

The cross-sectional average velocity of the river stream was estimated from the travel time difference data (obtained along the sound paths) which cover the channel cross-section. Moreover, the cross-sectional average salinity was estimated using the FAT data such as sound speed data, ray simulation results and the temperature data by the *C–T* sensors. This suggests that the freshwater discharge in tidal rivers can also be determined by the FAT system after separating the salt water component.

The water discharge, temperature and salinity determined from the FAT system were corroborated those obtained from the arrayed ADCPs and *C–T* sensors. This means that all of these environmental factors are observational targets of the FAT system.

Acknowledgements

We would like to thank Dr. Noriaki Gohda of Hiroshima University/Aqua Environmental Monitoring Limited Liability Partnership (AEM-LLP) for the strong support in field works and data processing. This study is supported by a fund from "the Construction Technology Research and Development Program of the Ministry of Land, Infrastructure, Transport and Tourism of Japan", and "the River Fund".

References

Catherine, A.R., DeRose, J.B., 2004. Investigation of hydroacoustic flow-monitoring alternatives at the Sacramento river at Freeport, California, results of the 2002-2004 pilot study.

Chiu, C.-L., Hsu, S.-M., 2006. Probabilistic approach to modeling of velocity distributions in fluid flows. Journal of Hydrology 316, 28–42.

Chiu, C.-L., Hsu, S.-M., Tung, N.-C., 2005. Measuring real-time streamflow using emerging technologies: radar, hydroacoustics, and the probability concept. Journal of Hydrology 357, 1–10.

Dushaw, B.D., Colosi, J.A., 1998. Ray tracing for ocean acoustic tomography. Technical memorandum, Applied Physics Laboratory, University of Washington (TM 3-98). 31 pp.

Maghrebi, M.F., 2006. Application of the single point measurement in discharge estimation. Advances in Water Resources 29 (10), 1504–1514.

Medwin, H., 1975. Speed of sound in water: a simple equation for realistic parameters. Journal Acoustical Society of America 58, 1318.

Shima, Y., Shiigai, H., Tamai, N., 1964. Salt wedge on inclined river bed. In: Annual meeting of JSCE. 2 pp.

Simon, M.K., Omura, J.K., Levitt, B.K., 1985. Spread Spectrum Communications Handbook. McGraw-Hill, New York. 423 pp.

Simpson, J.H., Brown, J., Matthews, J., Allen, G., 1990. Tidal straining, density currents, and stirring in the control of estuarine stratification. Estuaries 13 (2), 125–132.

Sloat, J.V., Gain, W.S., 1995. Application of acoustic velocity meters for gaging discharge of three low-velocity tidal streams in the St. John River Basin, Northeast Florida. US Geological Survey, Water-Resources Investigations Report, 95-4230. 26 pp.

Wang, F., Huang, H., 2005. Horizontal acoustic doppler current profiler (H-ADCP) for real-time open channel flow measurement: flow calculation model and field validation. In: XXXI IAHR CONGRESS, Seoul, Korea, pp. 319–328.

Zheng, H., Yamaoka, H., Gohda, N., Noguchi, H., Kaneko, A., 1998. Design of the acoustic tomography system for velocity measurement with an application to the coastal sea. Journal—Acoustical Society of Japan (E) 19, 199–210.